CHEMISTRY
A EUROPEAN JOURNAL

DOI: 10.1002/chem.200800327

# Supramolecular Sensing with Phosphonate Cavitands

**Monica Melegari,[a] Michele Suman,[a] Laura Pirondini,[a] Davide Moiani,[a] Chiara Massera,[b] Franco Ugozzoli,[b] Elina Kalenius,[c] Pirjo Vainiotalo,[c] Jean-Christophe Mulatier,[d] Jean-Pierre Dutasta,[d] and Enrico Dalcanale*[a]**

*In memory of Dmitry M. Rudkevich*

**Abstract:** Phosphonate cavitands are an emerging class of synthetic receptors for supramolecular sensing. The molecular recognition properties of the third-generation tetraphosphonate cavitands toward alcohols and water at the gas–solid interface have been evaluated by means of three complementary techniques and compared to those of the parent mono- and diphosphonate cavitands. The combined use of ESI-MS and X-ray crystallography defined precisely the host–guest association at the interface in terms of type, number, strength, and geometry of interactions. Quartz crystal microbalance (QCM) measurements then validated the predictive value of such information for sensing applications. The importance of energetically equivalent multiple interactions on sensor selectivity and sensitivity has been demonstrated by comparing the molecular recognition properties of tetraphosphonate cavitands with those of their mono- and diphosphonate counterparts.

**Keywords:** cavitands · host–guest chemistry · mass spectrometry · molecular recognition · sensors

## Introduction

Molecular recognition at interfaces constitutes an important theme in contemporary supramolecular chemistry. Addressing this issue is essential both for basic knowledge and for practical applications. For example, in chemical sensing, selectivity is the key parameter in defining success or failure of a given sensor, together with ruggedness.[1]

Reliable methods to assess and predict the complexation properties of molecular receptors at interfaces are therefore in demand. Both in natural and synthetic receptors, the basic tenet of most molecular recognition phenomena is their operation in solution, in which general dispersion interactions largely cancel out in moving the substrate from the solvent to the receptor site and in which the entropic cost of binding is partly paid by solvent release in the bulk. The same does not hold for recognition processes involving gaseous species, for which general, nonspecific dispersion interactions predominate in moving to the liquid/solid state.[2] In developing highly selective gas sensors, achieving effective molecular recognition at the gas–solid interface is therefore a demanding task that requires a fresh approach, both in terms of receptor design and characterization tools.[3]

The goal of this work is to provide a clear understanding of the parameters affecting molecular recognition of phosphonate cavitands at the gas–solid interface, with predicting values on their gas-sensing properties. To achieve this goal we set up an effective methodology for probing the molecular recognition properties of a given receptor at the gas–solid interface. It relies on the combined use of ESI-MS,

[a] Dr. M. Melegari, Dr. M. Suman, Dr. L. Pirondini, Dr. D. Moiani, Prof. E. Dalcanale
Dipartimento di Chimica Organica ed Industriale and
Unità INSTM, UdR Parma, Università degli Studi di Parma
Viale G.P. Usberti 17/a, 43100 Parma (Italy)
Fax: (+39) 0521-905-472
E-mail: enrico.dalcanale@unipr.it

[b] Dr. C. Massera, Prof. F. Ugozzoli
Dipartimento di Chimica Generale ed Inorganica
Chimica Analitica, Chimica Fisica
Università degli Studi di Parma
Viale G.P. Usberti 17/a, 43100 Parma (Italy)

[c] Dr. E. Kalenius, Prof. P. Vainiotalo
Department of Chemistry, University of Joensuu
P.O. Box 111, 80101 Joensuu (Finland)

[d] J.-C. Mulatier, Dr. J.-P. Dutasta
Laboratorie de Chimie
École Normale Supérieure de Lyon
CNRS, 46 Allée d'Italie, 69364 Lyon 07 (France)

Supporting information for this article is available on the WWW under http://www.chemeurj.org/ or from the author.

X-ray crystallography, and quartz crystal microbalance (QCM)[1] measurements. ESI-MS and X-ray crystallography were employed for the evaluation of the complexation properties of the receptors in the gas phase and solid state, respectively. They provide precise information on the type, number, strength, and geometry of the weak interactions responsible for the host–guest associations. The predictive value of such information for gas–solid interactions is validated by coating QCM transducers with the receptors and by exposing them to the analytes. By comparing the QCM responses of different receptors, the contributions of specific and nonspecific interactions can be dissected.

## Results and Discussion

The compounds used in the present work are the phosphonate cavitands shown below. They present an open, conformationally rigid cavity, delimited by one (Mi), two (ABii/ACii/ACio), or four (Tiiii) phosphonate bridging groups at the upper rim.[4]

In previous studies we have shown that the key factors affecting the sensing performances of mono- and diphosphonate cavitands toward alcohols are:

1) The simultaneous presence of hydrogen bonding with one of the P=O groups and CH–π interactions with the π-basic cavity, which requires an inward (i) orientation of the P=O bridges.[5]
2) A rigid cavity that provides a permanent free volume for the analyte around the inward facing P=O groups, pivotal for effective hydrogen bonding.[6]
3) The presence of two energetically equivalent hydrogen-bonding options available to the analyte in the case of AB/AC derivatives.[7]

The last factor suggests that increasing the number of convergent P=O groups in the cavitand should enhance alcohol complexation at the gas-solid interface.

To this purpose we prepared and tested third-generation cavitand receptors presenting four inward facing P=O bridges and compared them with their mono- and diphosphonate analogues, representing the first- and second-generation species, respectively. The corresponding tetrathiophosphonate cavitand TSiiii[$C_{11}H_{23}$,H,Ph] was also prepared to test the influence of hydrogen bonding on the sensing responses.

**Synthesis**: Cavitands Mi[$C_{11}H_{23}$,H,Ph],[4] ABii[$C_{11}H_{23}$,H,Ph],[6] and TSiiii[$C_{11}H_{23}$,H,Ph][8] were prepared following reported procedures. The Tiiii[$C_{11}H_{23}$,H,Ph] and Tiiii[H,$CH_3$,$CH_3$] cavitands were prepared according to the procedure reported in reference [9]. The preparation of the AC–diphosphonate cavitands ACii[H,$CH_3$,Ph] and ACio[H,$CH_3$,Ph] followed a two-step synthesis, in which partial methylene bridging of the starting resorcinarene was performed first, leaving the phosphonate bridging as last step (see Scheme S1, in the Supporting Information). The removal of the alkyl "feet" at the lower rim requires the presence of a methyl group in the 2-position of the starting resorcinol to avoid polymerization in the acid-catalyzed resorcinarene condensation reaction with formaldehyde.[10] Therefore all cavitands prepared for crystal structure studies have four methyl substituents at the upper rim.

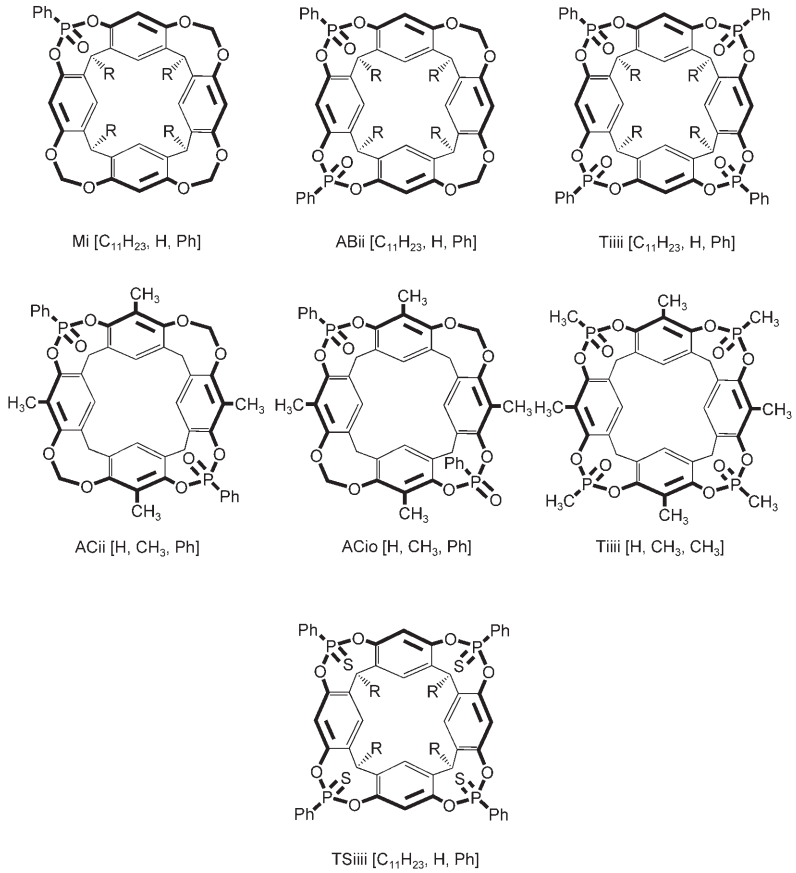


### Solid-state studies

*ACii/ACio cavitands*: Mono- and diphosphonate cavitands present a totally different behavior as receptor layers for alcohols in mass sensors according to the relative orientation of the P=O bridges. A single

  

P=O group pointing outward is sufficient to switch off the sensor responses.[5] Ideally, this remarkable difference should be reflected in the crystal structure of the respective alcohol complexes. Moreover, in the case of diphosphonate cavitands, the presence of a second inward facing P=O group enhances the sensor responses, independently from the relative position of the two moieties. The additional converging P=O group offers a second energetically and geometrically equivalent hydrogen bond to the guest, as revealed by the crystal structure of the ABii[$C_2H_5$,H,Ph]·MeOH complex for the AB isomer.[7] Whether or not this behavior is also followed by the AC isomer remains to be proven. Compact cavitands ACii-[H,$CH_3$,Ph] and ACio[H,$CH_3$,Ph] were synthesized to clarify their interaction mode with alcohols, removing the R substituents at the lower rim to facilitate single-crystal formation.

The crystals were obtained from a liquid diffusion of EtOH into a solution of the cavitands in $CH_2Cl_2$. The structure of the ACii[H,$CH_3$,Ph]·EtOH complex is shown in Figure 1. The ethanol molecule is located inside the cavitand

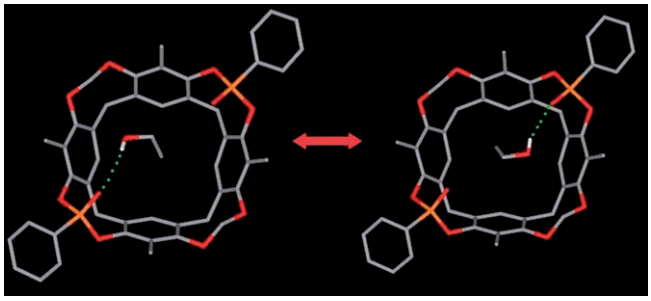

Figure 1. Molecular structure of the ACii[H,$CH_3$,Ph]·EtOH complex showing the two orientations of the hydroxyl hydrogen atoms (color code: P, orange; O, red; C, grey; H, white). The hydrogen atoms not involved in hydrogen bonding are omitted for clarity.

with its methyl group forming weak CH–π interactions with the aromatic walls of the cavity. The complex is further stabilized by the hydrogen bond between the OH group and the P=O moieties. As observed in the ABii-[H,$CH_3$,Ph]·MeOH case, the probability of interaction is maximized: the solvent is disordered with 50% probability over two equivalent orientations, thus forming alternatively a hydrogen bond with each of the two opposite P=O groups (O···O=P 2.795(3) Å). Therefore there is no difference in the binding mode in the solid state between AB and AC isomers, despite of the different spatial orientation of the P=O groups, as reflected in their comparable responses as sensors.[7]

The crystals of cavitand ACio[H,$CH_3$,Ph] (Figure 2) were grown under the same conditions of those of complex ACii-[H,$CH_3$,Ph]·EtOH. The phenyl ring pointing inside the cavity prevents any solvent inclusion, so that the disordered ethanol and dichloromethane molecules can only fill the empty spaces in the crystal lattice.

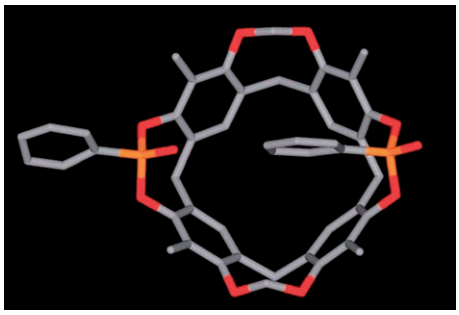

Figure 2. Molecular structure of one of the two symmetry independent cavitands in 2 ACio[H,$CH_3$,Ph]·EtOH·$CH_2Cl_2$ (color code: P, orange; O, red; C, grey). The hydrogen atoms and the solvent molecules in the lattice are omitted for clarity.

It is interesting to note that the ethanol molecules in the lattice (see Figure S1, Supporting Information) do not generate any hydrogen-bonding interaction with the P=O group oriented outside the cavity. Also for the ACio[H,$CH_3$,Ph] isomer, crystallographic data are in agreement with sensors measurements, showing a reduced affinity toward alcohols.

*Tiiii cavitands*: The influence of multiple hydrogen-bond acceptor sites on alcohol complexation has been assessed by synthesizing tetraphosphonate cavitands, with all four P=O bridges pointing into the cavity. Cavitand Tiiii[H,$CH_3$,$CH_3$] was specially synthesized for crystal structure determinations. Figure 3 shows the molecular structure of the

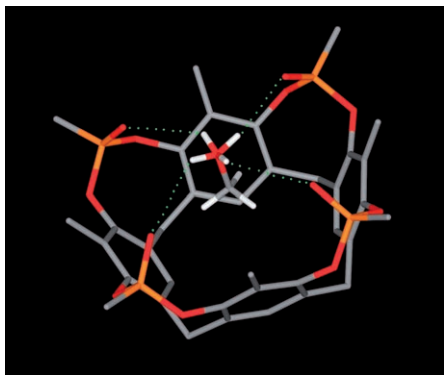

Figure 3. Molecular structure of the Tiiii[H,$CH_3$,$CH_3$]·MeOH complex showing the four orientations of the hydroxyl hydrogen atoms (color code: P, orange; O, red; C, grey; H, white). The hydrogen atoms not involved in the weak interactions are omitted for clarity.

Tiiii[H,$CH_3$,$CH_3$]·MeOH complex. The complex crystallizes in the tetragonal *P*4/*n* space group, with the methanol C–O bond lying on the fourfold axis, so that the methanol hydrogen atoms are statistically disordered over four different orientations. The alcohol interacts with the cavity through three CH–π interactions involving the methyl group and the aromatic rings of the cavitand (the CH···centroid distances span from 2.845(7) to 3.060(7) Å) and forming weak hydrogen bonds between the hydroxyl group and the phosphonate

  

moieties at the upper rim (MeOH···O=P 3.059(6) Å; Figure S2, Supporting Information).[11] Due to its statistical disorder around the fourfold axis, the methanol can switch among four different but isoenergetic triplets of CH···π interactions with the host cavity and at the same time it can also switch among four different isoenergetic MeOH···O=P attractive interactions with the host, leading to an entropic stabilization of the complex.

**Gas-phase studies**: No ethanol complexes were formed in the gas phase with cavitands presenting one or two P=O groups directed outward from the cavity.[12] These results clearly indicate that the cooperativity between hydrogen bonding and cavity inclusion is essential for complexation. The outward facing P=O are ineffective in hydrogen bonding both in the solid state and in the gas phase. Therefore ESI-MS competition experiments were restricted to all inward facing P=O/P=S cavitands to estimate their relative affinity toward ethanol. All competition experiments were carried out in 1:1 ethanol/acetonitrile solvent mixtures containing equimolar amounts of two cavitands. Mean intensities of ethanol complexes formed by Mi[$C_{11}H_{23}$,H,Ph] versus ABii[$C_{11}H_{23}$,H,Ph], and ABii[$C_{11}H_{23}$,H,Ph] versus Tiiii[$C_{11}H_{23}$,H,Ph] are plotted in Figure 4. The results imply that the thermodynamic stability of the complexes strongly depends on the number of P=O groups pointing into the cavity.

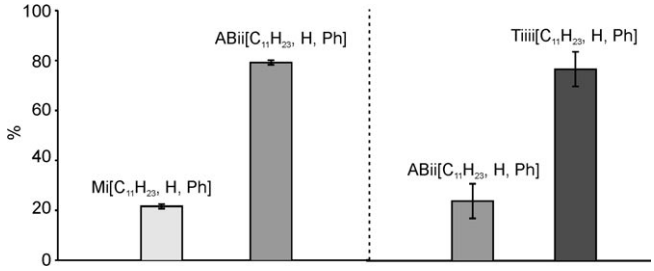


Figure 4. Mean intensities of the ethanol complexes obtained in competition experiments for the pairs Mi/ABii and ABii/Tiiii.

Under the same conditions, cavitand TSiiii[$C_{11}H_{23}$,H,Ph] did not form complexes with alcohols, due to the reduced hydrogen-bond acceptor ability of the P=S group compared to the P=O analogue.[13] The relative kinetic stability of all three ethanol complexes studied in competition experiments has been assessed by means of CID (collision induced dissociation) MS/MS experiments. Ethanol complexes of all cavitands dissociated producing the protonated cavitand $[M+H]^+$. The results shown in Figure 5 clearly indicate that also the kinetic stability of the ethanol complexes is directly related to the number of inward facing P=O groups present in the cavitand. ESI-MS experiments underline the importance of multiple hydrogen-bonding options available to the guest for effective complexation in the gas phase.

It is important to stress that the ESI-MS results are not only supportive, but also complementary to the solid-state

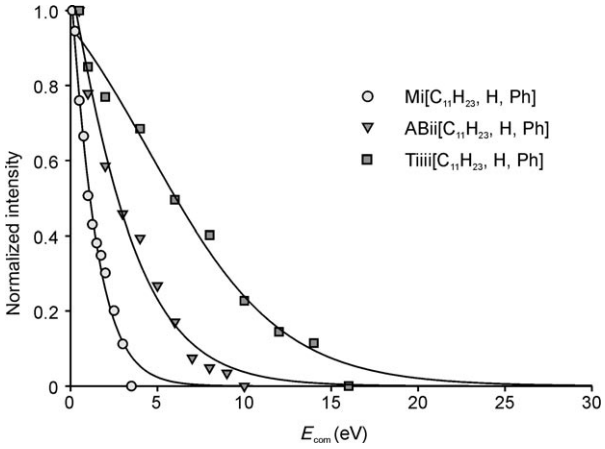


Figure 5. Dissociation (CID) of the ethanol complexes of Mi[$C_{11}H_{23}$,H,Ph], ABii[$C_{11}H_{23}$,H,Ph] and Tiiii[$C_{11}H_{23}$,H,Ph]. Normalized intensities as a function of activation energy in eV.

ones. The former gives an estimate of the relative thermodynamic and kinetic stability of the complexes as function of the number of inward directed P=O groups present, which cannot be inferred from the latter.

**QCM measurements**: Cavitands Mi[$C_{11}H_{23}$,H,Ph], ABii[$C_{11}H_{23}$,H,Ph], Tiiii[$C_{11}H_{23}$,H,Ph], TSiiii[$C_{11}H_{23}$,H,Ph], and reference polymer polyepichlorohydrin (PECH) were deposited by spin coating on both sides of a 10 MHz QCM transducer[14] and exposed to vapors of $C_1$–$C_4$ linear alcohols at different concentrations. The presence of long alkyl feet at the lower rim is essential to impart permeability to the layer.[3d] Comparison of the responses of the different coatings to MeOH vapors (Figure 6) highlights the positive effect of the number of inward facing P=O units on the sensor performances, as predicted.

The dependence of the sensor responses on hydrogen bonding is evidenced by comparing the behavior of Tiiii[$C_{11}H_{23}$,H,Ph] and TSiiii[$C_{11}H_{23}$,H,Ph] (Figure 7a). The latter behaves similarly to the unspecific polymeric coating PECH (Figure 7b). The structural similarity of the two cavitands allows a proper comparison of the sensor data, with-

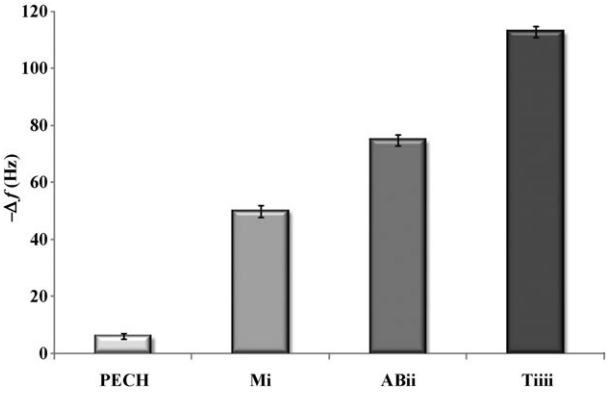


Figure 6. Selectivity patterns of cavitands Mi[$C_{11}H_{23}$,H,Ph], ABii[$C_{11}H_{23}$,H,Ph], Tiiii[$C_{11}H_{23}$,H,Ph], and polymer PECH to methanol at 1500 ppm.

  

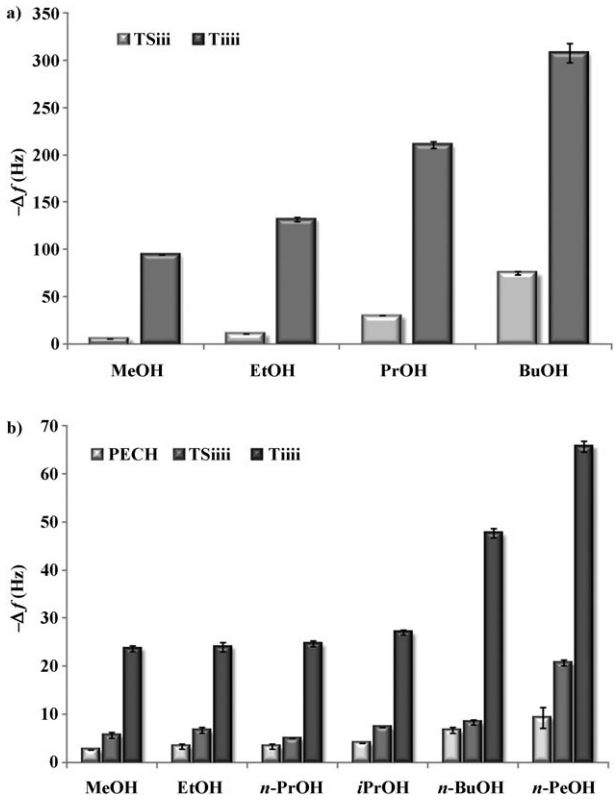


Figure 7. a) Responses of Tiiii[$C_{11}H_{23}$,H,Ph] and TSiiii[$C_{11}H_{23}$,H,Ph] to $C_1$–$C_4$ linear alcohols (1500 ppm each); b) responses of cavitands Tiiii[$C_{11}H_{23}$,H,Ph], TSiiii[$C_{11}H_{23}$,H,Ph], and polymer PECH to $C_1$–$C_5$ alcohols (25 ppm each).

out any bias due to different solid-state packing and coating morphology. Substitution of the four P=O groups with the P=S analogues strongly reduces the responses across the entire alcohol series, in line with ESI-MS data. The increased weight of dispersion interactions, associated with alcohol chain length, determines the general enhancement of the responses exhibited by both cavitands. This effect is particularly pronounced at high alcohol concentrations at which the layer is saturated (1500 ppm, Figure 7a). Nevertheless, the progressive dilution of specific responses is less evident at low analyte concentrations (25 ppm, Figure 7b), at which the energetically favorable cavity inclusions dominate.[6] A significant enhancement of the responses was only observed for *n*-butanol and *n*-pentanol, indicating that nonspecific extra cavity physisorption contribute significantly to the overall QCM response. In all other cases the response is comparable, suggesting that the inclusion mode is the same for short-chain alcohols.

The threshold value for alcohol detection has been determined for the most sensitive Tiiii[$C_{11}H_{23}$,H,Ph] in the case of ethanol in the 5–100 ppm regime (see Figure S3, Supporting Information). With a reproducible response of $8 \pm 0.6$ Hz at 5 ppm and a noise level of $\pm 1$ Hz for 10 MHz transducers, the lower limit of ethanol detection can be estimated in 2 ppm.

So far, the proposed methodology has shown the ability to predict the trend in the sensor responses for the cavitands, not for the analytes. The influence of dispersion interactions on the QCM responses for long-chain alcohols jeopardizes the identification of a clear trend in alcohol detection.

**The water case**: A closer match between prediction and experiment has been achieved in the case of water, an analyte which does not experience dispersion interactions.

The QCM data (Figure 8) show that TSiiii[$C_{11}H_{23}$,H,Ph] and Mi[$C_{11}H_{23}$,H,Ph] coatings are almost insensitive to water and that the response of Tiiii[$C_{11}H_{23}$,H,Ph] is twice

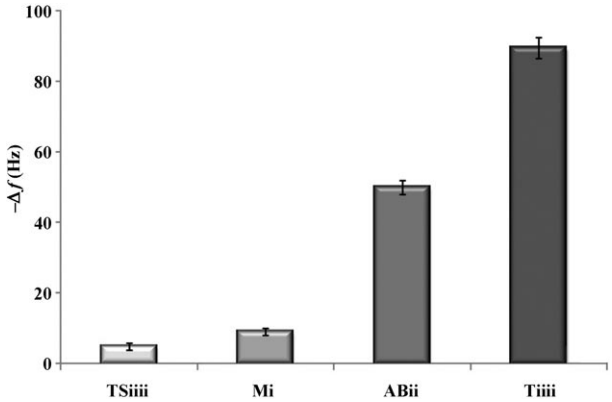


Figure 8. Selectivity patterns of cavitands TSiiii[$C_{11}H_{23}$,H,Ph], Mi[$C_{11}H_{23}$,H,Ph], ABii[$C_{11}H_{23}$,H,Ph], and Tiiii[$C_{11}H_{23}$,H,Ph] to water (230 ppm).

that of ABii[$C_{11}H_{23}$,H,Ph]. The same trend is present in the gas phase: TSiiii[$C_{11}H_{23}$,H,Ph] and Mi[$C_{11}H_{23}$,H,Ph] do not form any complex with water, while ABii[$C_{11}H_{23}$,H,Ph] forms a protonated $[M+H+H_2O]^+$ complex and Tiiii[$C_{11}H_{23}$,H,Ph] a protonated $[M+H+2H_2O]^+$ complex. The composition of these complexes was verified by a CID experiment (Figure 9).

The crystal structure of the Tiiii[H,$CH_3$,$CH_3$]·2 $H_2O$ complex, grown from trifluoroethanol, supports the complex stoichiometry indicated by the gas-phase experiments[15] and reveals the preferred host–guest hydrogen-bonding pattern (Figure 10, see also Figure S4, Supporting Information). The two water molecules are involved in a zig-zag chain of hydrogen bonds with the two distal P=O groups, instead of binding each of them to a vicinal P=O couple. Therefore, in the absence of nonspecific dispersion interactions, the binding mode stoichiometry is fully reflected in the corresponding mass-sensor responses (Figure 8). Such level of definition of host–guest interactions at the gas–solid interface is unprecedented, allowing reliable predictivity in sensor responses for the analyte/receptor pair.

## Conclusion

The third-generation tetraphosphonate cavitand receptors have been prepared and the corresponding mass sensors

  

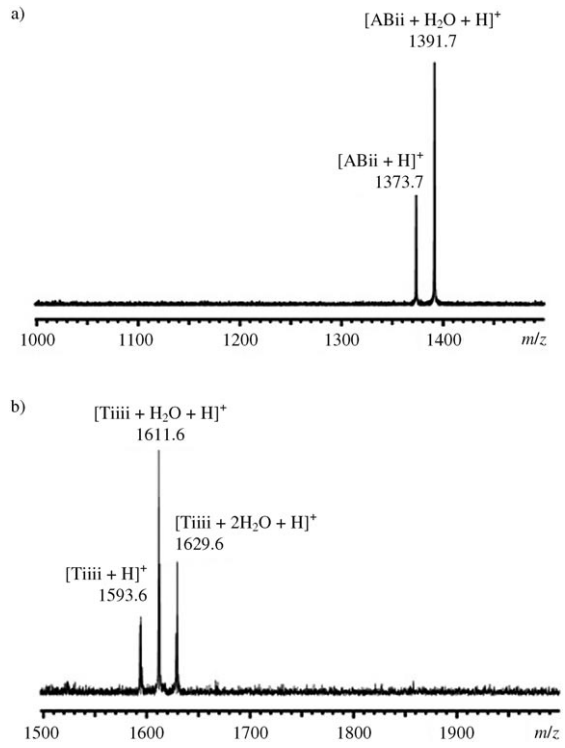


Figure 9. a) CID spectrum ($E_{com}=1.0$ eV) of pre-isolated *m/z* 1391.7. Measured from solution containing ABii[$C_{11}H_{23}$,H,Ph] and 2.5% water in ACN; b) CID spectrum ($E_{com}=1.0$ eV) of pre-isolated *m/z* 1629.6. Measured from solution containing Tiiii[$C_{11}H_{23}$,H,Ph] and 10% water in ACN.

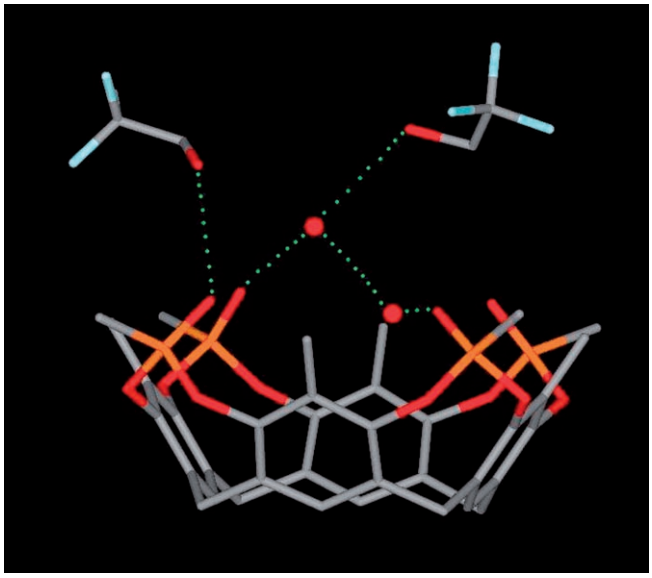

Figure 10. Molecular structure of the Tiiii[H,$CH_3$,$CH_3$]·2$CF_3CH_2OH$·2$H_2O$ complex showing the hydrogen-bond interactions (color code: P, orange; O, red; C, grey; H, white; F, light blue). The hydrogen atoms are omitted for clarity.

tested in their ability to detect alcohols and water. The alcohols complexation both in the solid state and in the gas phase is driven by the cooperative effect of hydrogen bonding and CH–π interactions, made possible by the insertion of phosphonate bridges on top of a preorganized cavity. Neither interaction, taken alone, is sufficient for efficient complexation. QCM measurements showed that the third generation Tiiii cavitands outperforms the previous two (Mi, ABii/ACii) in terms of sensor responses. The results demonstrated that the entropic stabilization of host–guest complexes through energetically equivalent multiple interactions is a viable route to enhance sensitivity and selectivity in mass sensors, while retaining full reversibility.

In conclusion, the combined use of ESI-MS and crystallographic analyses allows us to anticipate the molecular recognition properties of cavitands at the gas–solid interface, when the dominant interactions in the two phases coincide. In the absence of dispersion interactions, this approach allows us to predict the trend in sensor responses of a given analyte–cavitand pair. The overall methodology is of wide applicability to many receptor–analyte pairs, allowing an easy and reliable evaluation of their molecular recognition potential at interfaces.

## Experimental Section

**Cavitands synthesis**

*Tiiii[$C_{11}H_{23}$,H,Ph]*: Dichlorophenylphosphate (1.23 mL, 7.96 mmol) and *N*-methylpyrrolidine (213 μL, 2.04 mmol) were added, under nitrogen, to a solution of undecyl-"footed" resorcinarene (2.0 g, 1.81 mmol) in anhydrous toluene (100 mL). The mixture was stirred at 112 °C for 5 h. After evaporation of the solvent, the crude product was purified by column chromatography ($SiO_2$, $CH_2Cl_2$/EtOH 9:1) to give the title compound as white solid (1.44 g, 50%). $^1$H NMR ($CDCl_3$, 300 MHz): $\delta=8.08$–7.98 (m, 8H; $POArH_o$), 7.60–7.53 (m, 12H; $POArH_m$+$POArH_p$), 7.29 (s, 4H; $ArH_{down}$), 6.97 (s, 4H; $ArH_{up}$), 4.78 (t, $^3J=7.6$ Hz, 4H; $RCHAr_2$), 2.37 (m, 8H; $CHCH_2R$), 1.43–1.25 (m, 72H; -$CH_2$-), 0.86 ppm (t, $^3J=6.9$ Hz, 12H; -$CH_3$); $^{31}$P NMR ($CDCl_3$, 162 MHz): $\delta=5.83$ ppm (s, POAr); ESI-MS: *m/z*: 1595.4 $[M+H]^+$, 1618.3 $[M+Na]^+$.

*Tiiii[H,$CH_3$,$CH_3$]*: Dichloromethylphosphate (1.46 mL, 16.17 mmol) and *N*-methylpyrrolidine (432 μL, 4.15 mmol) were added, under nitrogen, to a suspension of resorcinarene **1** (2.0 g, 3.67 mmol) in anhydrous dichlorobenzene (100 mL). The mixture was stirred at 140 °C for 24 h. After evaporation of the solvent, the crude product was purified by column chromatography ($SiO_2$, $CH_2Cl_2$/MeOH 8:2) to give the title compound as white solid (0.81 g, 28%). $^1$H NMR ($CDCl_3$/MeOD, 300 MHz): $\delta=6.99$ (s, 4H; $ArH_{down}$), 4.19 (d, $^2J=13$ Hz, 4H; $CH_{2eq}Ar_2$), 3.36 (d, $^2J=13$ Hz, 4H; $CH_{2ax}Ar_2$), 1.98 (s, 12H; $ArCH_3$), 1.81 ppm (d, $J_{H\text{-}P}=18$ Hz, 12H; $POCH_3$); $^{31}$P NMR ($CDCl_3$/MeOD, 162 MHz): $\delta=22.03$ ppm (s, $POCH_3$); ESI-MS: *m/z* (%): 785.3 (30) $[M+H]^+$, 823.3 (100) $[M+K]^+$.

*AC methylene dibridged resorcinarene*: Dibromomethane (0.14 mL, 1.93 mmol) and $K_2CO_3$ (512 mg, 3.70 mmol) were added to a solution of resorcinarene **1** (SI) (526 g, 0.966 mmol) in anhydrous DMA (80 mL). The mixture was stirred at 80 °C for 3 h. After evaporation of the solvent, the crude product was purified by column chromatography ($SiO_2$, hexane/acetone 7.5:2.5) to give the AC isomer as white solid (38 mg, 7%). $^1$H NMR ($CDCl_3$, 300 MHz): $\delta=7.08$ (s, 4H; $ArH_{down}$), 6.33 (brs, 4H; ArOH), 5.89 (d, $^2J=7$ Hz, 2H; O-$CH_{2out}$-O), 4.45 (d, $^2J=13$ Hz, 2H; $CH_{2ax}Ar_2$), 4.35 (d, $^2J=7$ Hz, 2H; O-$CH_{2in}$-O), 4.05 (d, $^2J=13$ Hz, 2H; $CH_{2ax}Ar_2$), 3.46 (d, $^2J=13$ Hz, 2H; $CH_{2eq}Ar_2$), 3.25 (d, $^2J=13$ Hz, 2H; $CH_{2eq}Ar_2$), 2.01 (s, 12H; $ArCH_3$); ESI-MS: *m/z* (%): 607.3 (100) $[M+K]^+$.

*ACii[H,$CH_3$,Ph] and ACio[H,$CH_3$,Ph]*: Dichlorophenylphosphate (20 μL, 0.142 mmol) and *N*-methylpyrrolidine (8 μL, 0.076 mmol) were added, under nitrogen, to a solution of AC methylene dibridged resorcinarene (38 mg, 0.067 mmol) in anhydrous toluene (33 mL). The mixture was

  

stirred at 112 °C for 5 h. After evaporation of the solvent, the crude product was purified by column chromatography ($SiO_2$, hexane/THF 5:5) to give the ACii isomer (7 mg, 13 %) and the ACio isomer (10 mg, 18 %) as a white solid.

*ACii*: $^1$H NMR ($CDCl_3$, 300 MHz): $\delta = 8.13$ (m, 4H; $POArH_o$), 7.66–7.56 (m, 6H; $POArH_m$ + $POArH_p$), 7.04 (s, 4H; $ArH_{down}$), 5.81 (d, $^2J = 7$ Hz, 2H; O-$CH_{2out}$-O), 4.71 (d, $^2J = 7$ Hz, 2H; O-$CH_{2in}$-O), 4.51 (d, $^2J = 13$ Hz, 2H; $CH_{2ax}Ar_2$), 4.45 (dd, $^2J = 13$ Hz, $J_{H\text{-}P} = 3$ Hz, 2H; $CH_{2ax}Ar_2$), 3.46 (d, $^2J = 13$ Hz, 2H; $CH_{2eq}Ar_2$), 3.29 (d, $^2J = 13$ Hz, 2H; $CH_{2eq}Ar_2$), 2.15 ppm (s, 12H; $ArCH_3$); $^{31}$P NMR ($CDCl_3$, 162 MHz): $\delta = 6.61$ ppm (s, POAr); ESI-MS: *m/z* (%): 835.1 (100) $[M+Na]^+$.

*ACio*: $^1$H NMR ($CDCl_3$, 300 MHz): $\delta = 8.12$ (m, 4H; $POArH_o$), 7.69–7.60 (m, 3H; $POArH_m$ + $POArH_p$), 7.32 (m, 1H; POArH), 7.13 (s, 2H; $ArH_{down}$), 7.12 (s, 2H; $ArH_{down}$), 6.82 (m, 2H; POArH), 6.72 (m, 2H; POArH), 5.70 (d, $^2J = 7$ Hz, 2H; O-$CH_{2out}$-O), 4.72 (d, $^2J = 13$ Hz, 1H; $CH_{2ax}Ar_2$), 4.51 (d, $^2J = 13$ Hz, 2H; $CH_{2ax}Ar_2$), 4.42 (dd, $^2J = 13$ Hz, $J_{H\text{-}P} = 3$ Hz, 1H; $CH_{2ax}Ar_2$), 3.91 (d, $^2J = 7$ Hz, 2H; O-$CH_{2in}$-O), 3.58 (d, $^2J = 13$ Hz, 1H; $CH_{2eq}Ar_2$), 3.51 (d, $^2J = 13$ Hz, 1H; $CH_{2eq}Ar_2$), 3.32 (d, $^2J = 13$ Hz, 2H; $CH_{2eq}Ar_2$), 2.08 (s, 6H; $ArCH_3$), 1.62 ppm (s, 6H; $ArCH_3$). $^{31}$P NMR ($CDCl_3$, 162 MHz): $\delta = 8.19$ (s, 1P, POAr), 4.32 ppm (s, 1P; POAr); ESI-MS: *m/z* (%): 835.1 (100) $[M+Na]^+$.

**Crystal structures**: The crystal structure of complexes ACii-[H,$CH_3$,Ph]·EtOH, 2 ACio[H,$CH_3$,Ph]·EtOH·$CH_2Cl_2$, Tiiii[H,$CH_3$,$CH_3$]·MeOH and Tiiii[H,$CH_3$,$CH_3$]·2 $CF_3CH_2OH$·2 $H_2O$ were determined by single-crystal X-ray diffraction methods. Crystallographic and experimental details for the structures are summarized in Tables S1 and S2 in the Supporting Information. Intensity data and cell parameters were recorded at room temperature on a Bruker AXS Smart 1000 single-crystal diffractometer, equipped with a CCD area detector with graphite monochromated $Mo_{K\alpha}$ radiation. The structures were solved by direct methods by using the SIR97 program[16] and refined on $F_o^2$ by full-matrix least-squares procedures, with the SHELXL-97 program.[17] Both programs were used in the WinGX suite.[18] The data reductions were performed by using the SAINT[19] and SADABS[20] programs. All the non-hydrogen atoms were refined with anisotropic atomic displacements, with the exclusion of the disordered ethanol guest in ACii[H,$CH_3$,Ph]·EtOH, of two carbon atoms of one phenyl ring and of the disordered ethanol and dichloromethane solvent in 2 ACio[H,$CH_3$,Ph]·EtOH·$CH_2Cl_2$, of the methanol guest in Tiiii[H,$CH_3$,$CH_3$]·MeOH, and of the trifluoroethanol and water molecules in Tiiii[H,$CH_3$,$CH_3$]·2 $CF_3CH_2OH$·2 $H_2O$. The hydrogen atoms were included in the refinement at idealized geometries (C–H 0.95 Å) and refined "riding" on the corresponding parent atoms. The weighting scheme used in the last cycle of refinement was $w = 1/[\sigma^2F_o^2 + (0.1535P)^2]$, $w = 1/[\sigma^2F_o^2 + (0.1155P)^2]$, $w = 1/[\sigma^2F_o^2 + (0.1305P)^2]$, and $w = 1/[\sigma^2F_o^2 + (0.2181P)^2]$ with $P = (F_o^2 + 2F_c^2)/3$ for ACii[H,$CH_3$,Ph]·EtOH, 2 ACio[H,$CH_3$,Ph]·EtOH·$CH_2Cl_2$, Tiiii[H,$CH_3$,$CH_3$]·MeOH, and Tiiii[H,$CH_3$,$CH_3$]·2 $CF_3CH_2OH$·2 $H_2O$, respectively.

CCDC-678546 (ACii[H,$CH_3$,Ph]·EtOH), 678547 (2 ACio[H,$CH_3$,Ph]·EtOH·$CH_2Cl_2$), 655612 (Tiiii[H,$CH_3$,$CH_3$]·MeOH), and 655313 (Tiiii[H,$CH_3$,$CH_3$]·2 $CF_3CH_2OH$·2 $H_2O$) contain the supplementary crystallographic data for this paper. These data can be obtained free of charge from The Cambridge Crystallographic Data Centre via www.ccdc.cam.ac.uk/data_request/cif. Geometric calculations were performed with the PARST97 program.[21]

**ESI-MS studies**: Mass spectrometry experiments were performed with the BioApex 47e Fourier transform ion cyclotron resonance mass spectrometer equipped with an Infinity™ cell, a passively shielded 4.7 T 160 mm bore superconducting magnet, and an external Apollo™ electrospray ionization source. The sample was introduced to a 70° off-axis sprayer (stainless steel metal capillary) through a syringe infusion pump at a flow rate of 1.5 μL min$^{-1}$. Room-temperature nitrogen ($N_2$) was used as a nebulizing and counter-current drying gas. The measurements and data handling were accomplished with Bruker XMASS software, version 6.0.2. More precise description of instrument and the parameters used have been published.[12] Cavitand concentration in samples was 2.0–4.0 μM. The samples for water complexation contained cavitand (2 μM), 1–20 % (v/v) $H_2O$, 0.5 % (v/v) acetic acid and ACN as a solvent. Competition experiments with cavitands were performed with a cavitand1/cavitand2 ratio of 1:1 in the presence of ethanol. Each experiment was carried out on five different samples and each sample was measured five times. The overall variance was calculated from the standard deviation of sampling and the standard deviation of the measurement ($s_{tot}^2 = s_1^2 + s_2^2$). In collision induced dissociation (CID) experiments, collisionally cooled precursor ions were isolated by the CHEF procedure.[22] Isolated ions were thermalized during 3.0 s delay, translationally activated by an on-resonance radio frequency (RF) pulse, and allowed to collide with pulsed argon background gas. Each spectrum was a collection of 32 scans.

**Sensors measurements**: Sensing measurements were performed using a 10 MHz AT-cut quartz. Cavitands films were deposited on gold electrode areas on both sides of the quartz transducers by spin-coating deposition technique. Each microbalance was coated with the same amount of cavitand, which was verified by measuring the frequency shift of $\Delta f = 20 \pm 0.5$ kHz on the final coated QCM. The measurement system (Gaslab 20.1; IFAK, Magdeburg) was equipped with a flow chamber, containing four coated quartz crystals, a reference quartz crystal, and a thermocouple. The temperature of the chamber was thermostated at $20 \pm 0.1$ °C. The QCM chamber was connected with two mass flow controllers (Brooks 5850S): one allowed control of the flow rate of alcohol mixture between 2 and 50 mL min$^{-1}$ and the other controlled the flow rate of pure nitrogen from 150 to 200 mL min$^{-1}$. The starting stream of $N_2$ ($200 \pm 2$ mL min$^{-1}$) was then replaced by a $N_2$ + alcohol mixture ($200 \pm 2$ mL min$^{-1}$); the $N_2$/alcohol ratio was imposed by the desired final alcohol concentration considering that the total amount of the stream had to be $200 \pm 2$ mL min$^{-1}$. After reaching of the flat characteristic plateau (equilibrium of the partition coefficient) the chamber was flushed with pure $N_2$ to restore the starting conditions. During the whole process the coated quartz crystal frequency was measured as a function of the time every 1 s. All measurements were repeated at least four times, with variations in response of less than 3 %. Alcohols used in low ppm measurements were supplied by SAPIO S.r.l. in gas cylinders with a certified concentration of in ppm. The graduated cylinders were prepared following the standard gravimetric procedure of the normative ISO 6142. In the case of high ppm measurements (1500 ppm) the organic vapors were generated by bubbling a stream of nitrogen carrier gas through the volatile liquids to produce a continuous steam saturated with vapor, the concentration of which depended on the vapor pressure of the liquid (values were obtained by experimental data interpolation[23]). This stream was diluted with nitrogen by the second mass flow controller to obtain the desired analyte concentration.

## Acknowledgements

This work was supported by MUR through Progetto Galileo (French-Italian exchange program to E.D. and J.P.D.) and by EU through NoE MAGMANet (3-NMP 515767-2). The instrumental facilities at the Centro Interfacoltà di Misure G. Casnati of the University of Parma were used. The financial support from the Magnus Ehrnrooth foundation and the MaBio project by the European Social Fund and the State provincial office of Eastern Finland, the Department of Education and Culture (E.K.) is also acknowledged.

[1] J. W. Grate, G. C. Frye, in *Sensors Update, Vol. 2* (Eds: H. Baltes, W. Göpel, J. Hesse), Wiley-VCH, Weinheim (Germany), **1996**, pp. 10–20.

[2] J. Janata, in *Principles of Chemical Sensors*, Plenum, New York (USA), **1989**.

[3] a) F. L. Dickert, H. Stathopulos, M. Reif, *Adv. Mater.* **1996**, *8*, 525–529; b) D. M. Rudkevich, *Angew. Chem.* **2004**, *116*, 568–581; *Angew. Chem. Int. Ed.* **2004**, *43*, 558–571; c) S. J. Dalgarno, P. K. Thallapally, L. J. Barbour, J. A. Atwood, *Chem. Soc. Rev.* **2007**, *36*, 236–245; d) L. Pirondini, E. Dalcanale *Chem. Soc. Rev.* **2007**, *36*, 695–706; e) A. G. Grechin, H.-J. Buschmann, E. Schollmeyer *Angew. Chem.* **2007**, *119, 6619–6621; Angew. Chem. Int. Ed.* **2007**, 46, 6499–6501; *Angew. Chem. Int. Ed.* **2007**, *46*, 6499–6501.

  

[4] For the nomenclature adopted for phosphonate cavitands see: R. Pinalli, M. Suman, E. Dalcanale, *Eur. J. Org. Chem.* **2004**, 451–462.
[5] R. Pinalli, F. F. Nachtigall, F. Uguzzoli, E. Dalcanale, *Angew. Chem.* **1999**, *111*, 2530–2533; *Angew. Chem. Int. Ed.* **1999**, *38*, 2377–2380.
[6] R. Paolesse, C. Di Natale, S. Nardis, A. Magagnano, A. D'Amico, R. Pinalli, E. Dalcanale, *Chem. Eur. J.* **2003**, *9*, 5388–5395.
[7] M. Suman, M. Freddi, C. Massera, F. Uguzzoli, E. Dalcanale, *J. Am. Chem. Soc.* **2003**, *125*, 12068–12069.
[8] B. Bibal, J. P. Declercq, J. P. Dutasta, B. Tinant, A.-G. Valade, *Tetrahedron* **2003**, *59*, 5849–5854.
[9] P. Delangle, J.-C. Mulatier, B. Tinant, J.-P. Declercq, J.-P. Dutasta, *Eur. J. Org. Chem.* **2001**, 3695–3704.
[10] H. Konishi, Y. Iwasaki, T. Okano, J. Kiji, *Chem. Lett.* **1989**, 1815–1816.
[11] G. R. Desiraju, T. Steiner, in *The Weak Hydrogen Bond*, Oxford University Press, Oxford (UK), **1999**, pp. 12–15.
[12] E. Ventola, P. Vainiotalo, M. Suman, E. Dalcanale, *J. Am. Soc. Mass Spectrom.* **2006**, *17*, 213–221.
[13] D. Reyntjens-Van Damme, T. Zeegers-Huyskens, *J. Phys. Chem.* **1980**, *84*, 282–285.
[14] The amount of material coated was controlled by measuring a frequency shift of $\Delta f = 20 \pm 0.05$ kHz on deposition of each layer.
[15] The MMFF-B3LYP/6–31G* computed structure in the gas phase is fully consistent with the crystal structure both in terms of complex stoichiometry and water binding mode (D. V. Dearden, E. Dalcanale, unpublished results).
[16] A. Altomare, M. C. Burla, M. Camalli, G. L. Cascarano, C. Giacovazzo, A. Guagliardi, A. G. Moliterni, G. Polidori, R. Spagna, *J. Appl. Crystallogr.* **1999**, *32*, 115–119.
[17] G. M. Sheldrick, SHELXL97, Program for Crystal Structure Refinement, University of Göttingen, Göttingen (Germany), **1997**.
[18] WinGX: L. J. Farrugia, *J. Appl. Crystallogr.* **1999**, *32*, 837–838.
[19] SAINT, Software Users Guide, 6.0, Bruker Analytical X-ray Systems, **1999**.
[20] G. M. Sheldrick, SADABS Area-Detector Absorption Correction, 2.03, University of Göttingen, Göttingen (Germany), **1999**.
[21] M. Nardelli, *J. Appl. Crystallogr.* **1996**, *29*, 296–300.
[22] L. J. De Koning, N. M. Nibbering, S. L. Van Orden, F. H. Laukien, *Int. J. Mass Spectrom. Ion Processes* **1997**, *165*/166, 209–219.
[23] R. H. Perry, D. W. Green, *Perry Chemical Engineers' Handbook*, 7th ed., McGraw-Hill, New York, **1997**.

Received: February 21, 2008
Published online: May 19, 2008

  